Supporting Information

Development of a NS-CDs/Fluorescein Ratiometric Fluorescent Sensor Integrated Smartphone Platform for Rapid and Specific Detection of Mn(VII) and Captopril

Chuntong Liu[a,c], Haiyan Qi[a]*, Jiayu Zhang[a], Jun Li[a,b], Tao Jing[a], Qiuying Li[a], Lixin Qiu[a] and Xiaochen Zhu[a]

[a] College of Chemistry and Chemical Engineering, Qiqihar University, Qiqihar, Heilongjiang 161006, P. R. China.

[b] Technology Innovation Center of Industrial Hemp for State Market Regulation, Qiqihar, Heilongjiang 161006, P. R. China.

[c] College of Arts and Sciences, Northeast Agricultural University, No. 600 Changjiang Road, Harbin 150030, China.

* Corresponding Authors E-mail: qhy120@sina.com (Haiyan Qi)

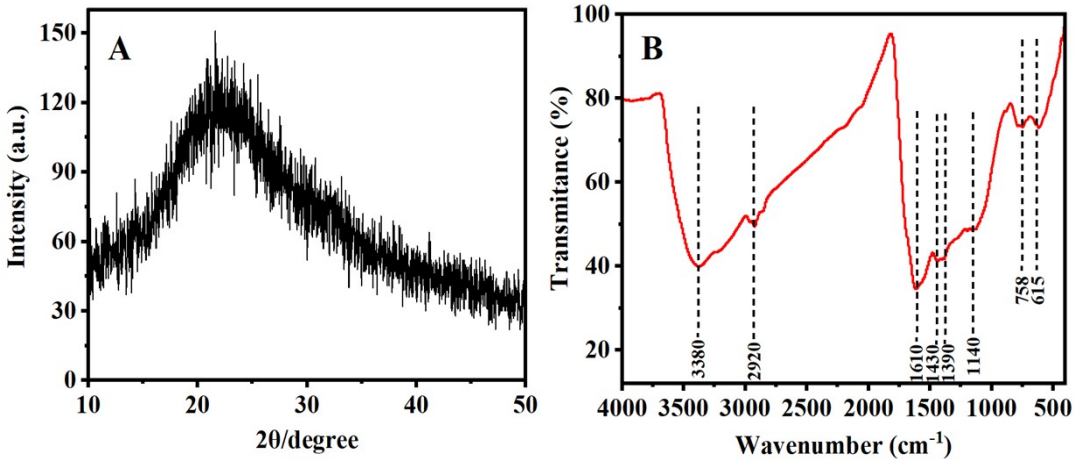

Figure S1. (A) X-ray diffraction (XRD) pattern of NS-CDs; (B) Fourier transform infrared (FTIR) spectroscopy of NS-CDs.

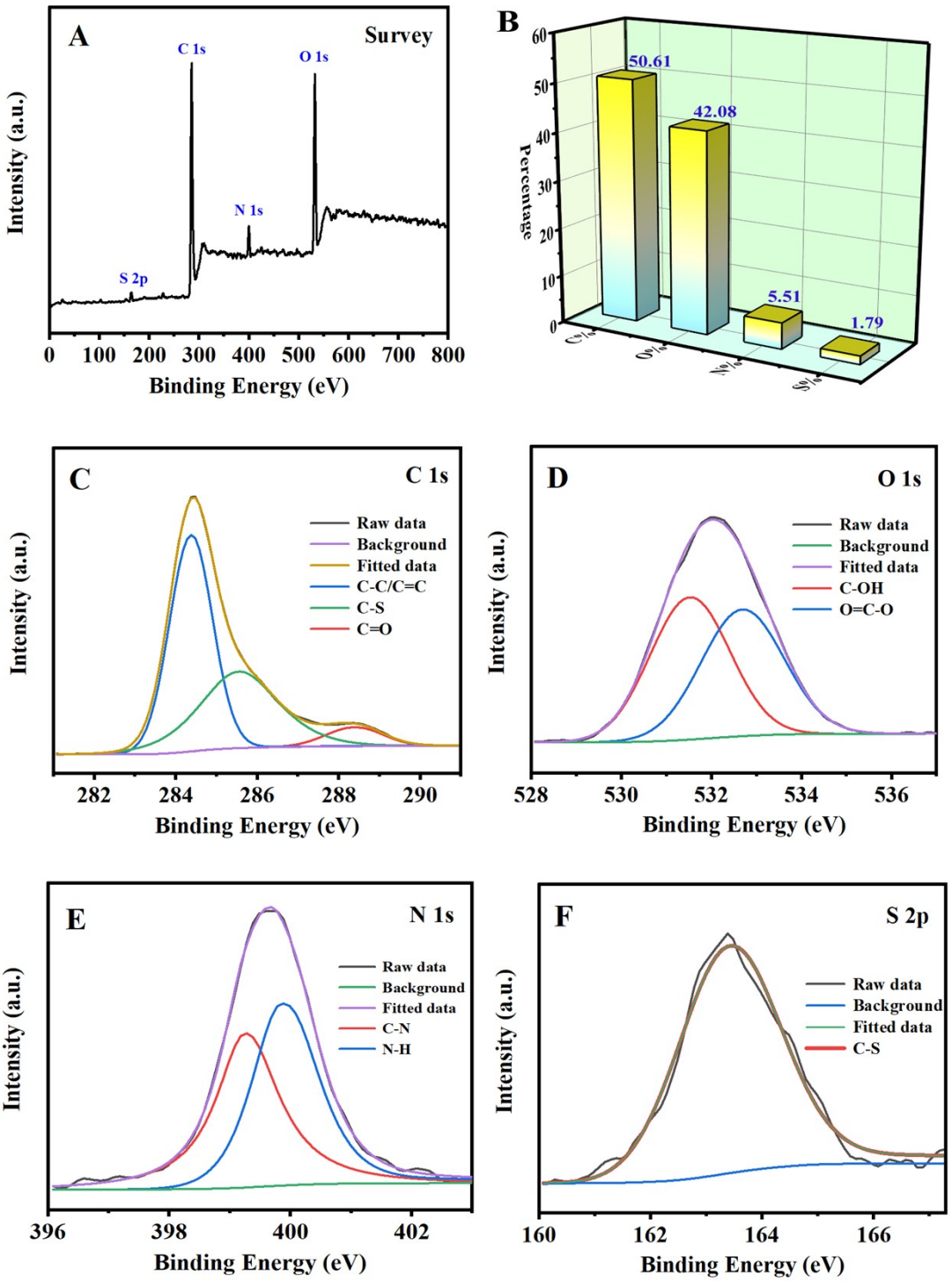

Figure S2. X-ray photoelectron spectroscopy (XPS) analysis of NS-CDs. (A) XPS survey scan of NS-CDs; (B) Element distribution of NS-CDs; High-resolution XPS spectra of (C) C1s, (D) O1s, (E) N1s, and (F) S2p of NS-CDs.

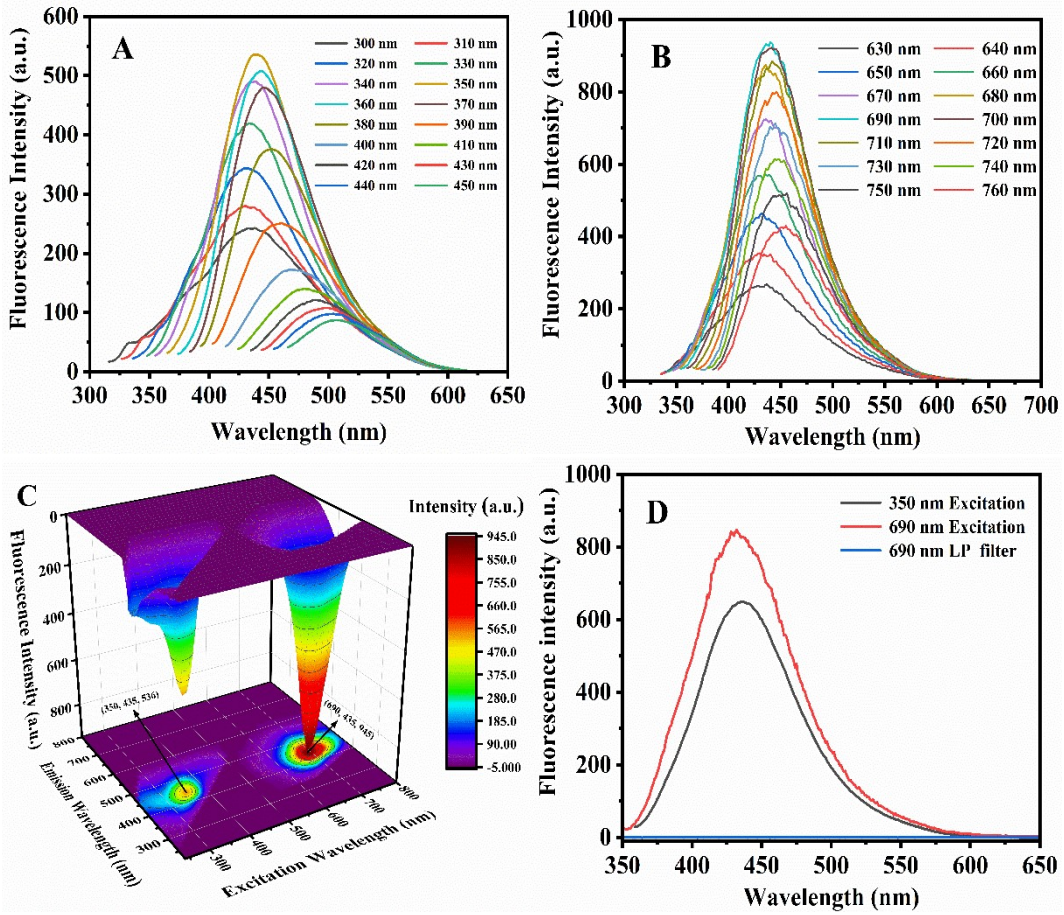

Figure S3. Fluorescence characterization of NS-CDs. (A) Emission spectra of NS-CDs excited at different short wavelengths; (B) Emission spectra of NS-CDs excited at different long wavelengths; (C) Excitation-emission 3D fluorescence matrix of NS-CDs within the full wavelength range; (D) Emission spectra of G-CDs at 690 nm before and after the addition of a long-pass (LP) filter

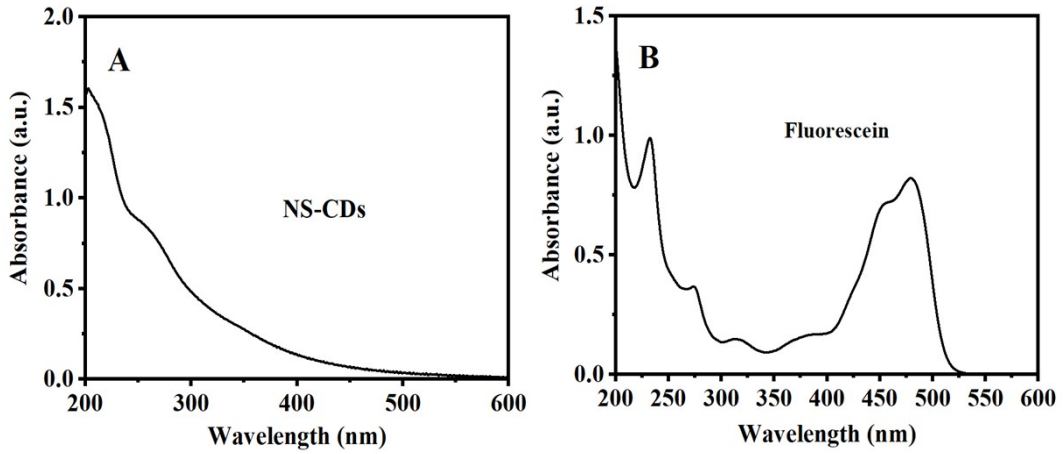

Figure S4. (A) UV-visible absorption spectrum of NS-CDs; (B) UV-visible absorption spectrum of fluorescein.

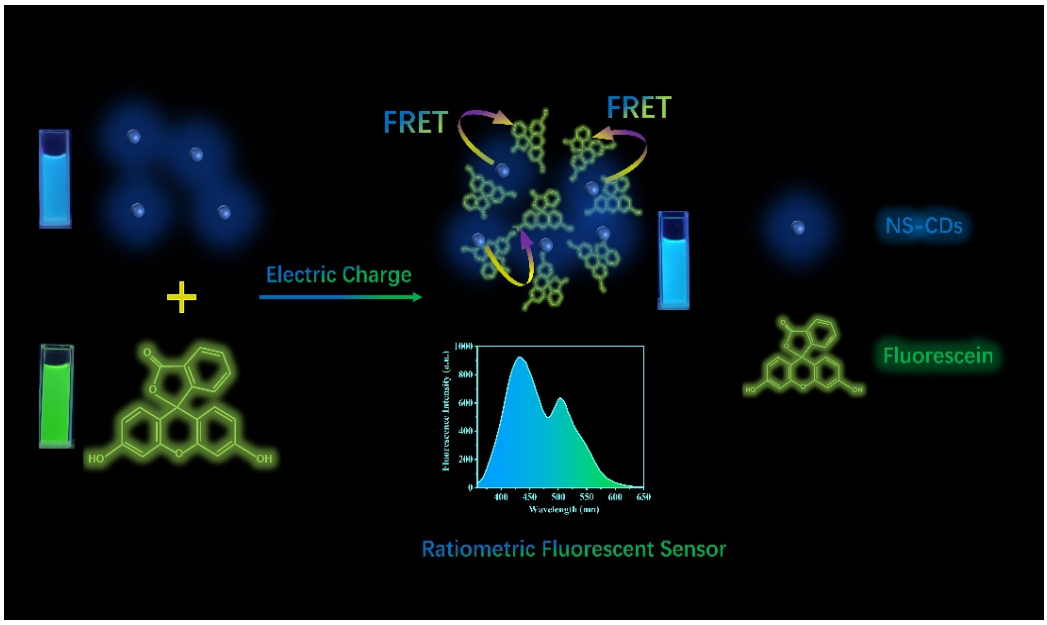

Figure S5. Mechanism of construction of NS-CDs/fluorescein ratio fluorescent sensor

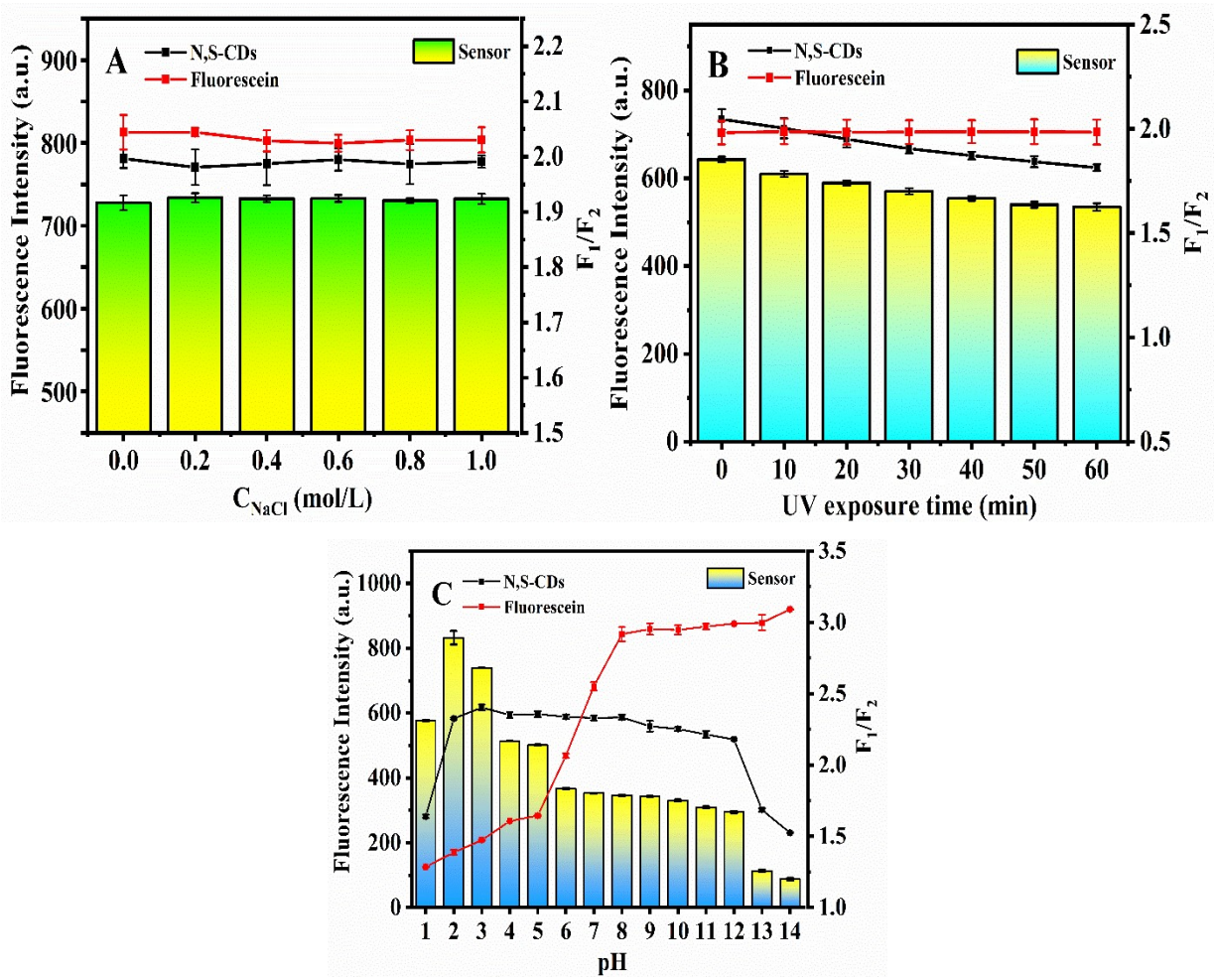

Figure S6. Characterization of the NS-CDs/fluorescein ratiometric fluorescent sensor. (A) Salt tolerance of the sensor; (B) Photostability of the sensor; (C) pH sensitivity of NS-CDs, fluorescein, and the NS-CDs/fluorescein ratio fluorescent sensor.

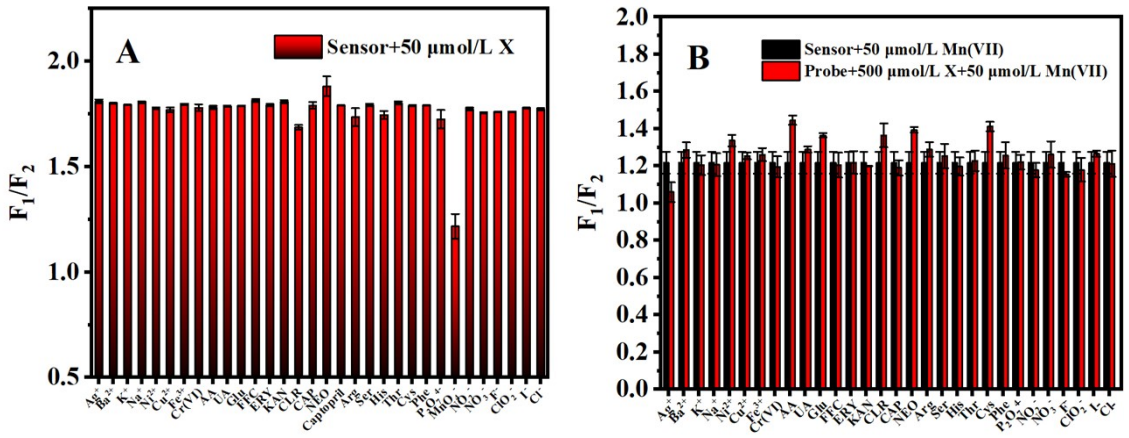

Figure S7. Specificity and selectivity of Mn(VII) detection using the NS-CDs/fluorescein ratiometric fluorescent sensor. (A) Selectivity of the sensor to different substances; (B) Interference of Mn (VII) detected by the sensor with other substances.

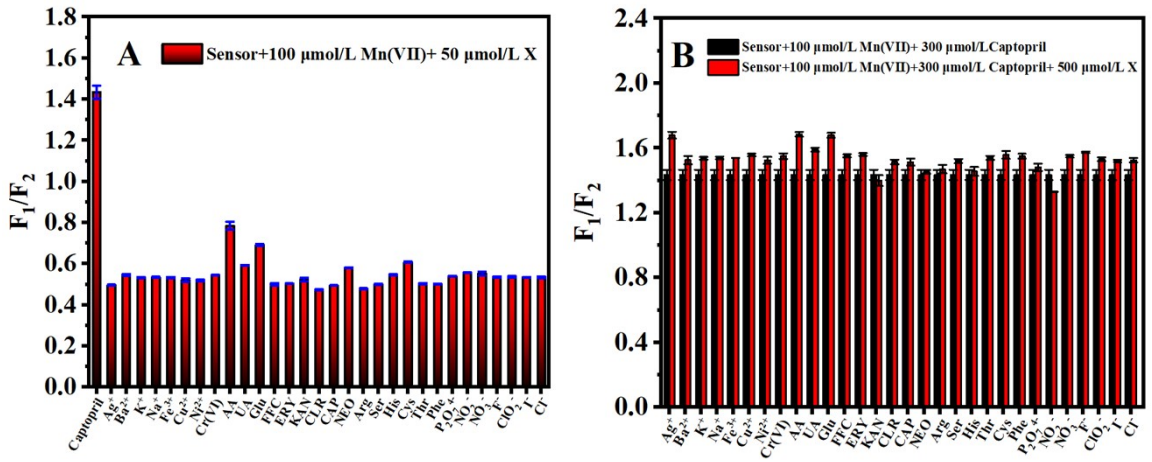

Figure S8. Specificity and Selectivity of captopril detection using the sensor/Mn(VII) system. (A) Selectivity of the sensor/Mn(VII) system to different substances; (B) Interference of captopril detected by the sensor/Mn(VII) system with other substances.

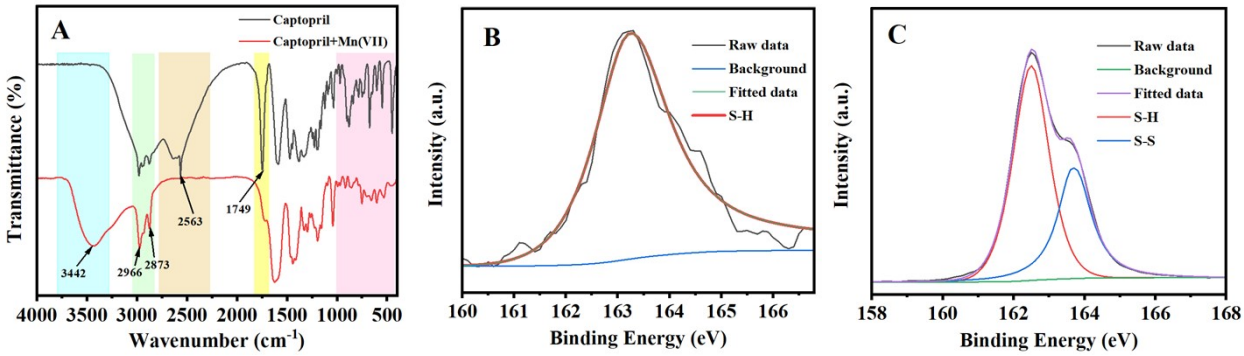

Figure S9. (A) IR spectra for captopril before and after adding Mn(VII); (B) S2p spectrum of captopril before joining Mn(VII); (C) S2p spectrum of captopril after adding Mn(VII).

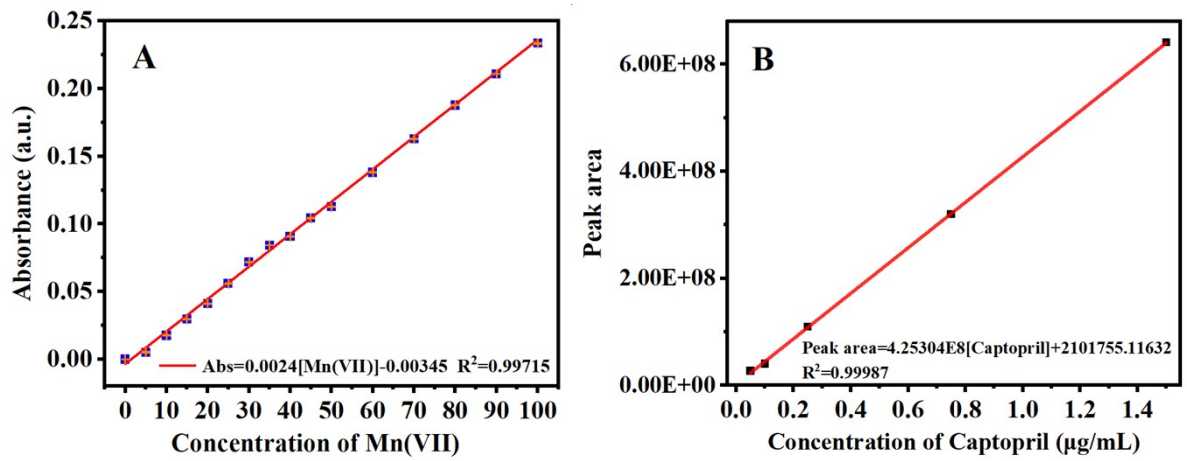

Figure S10. (A) UV-Vis spectra of Mn(VII) with various concentrations. (B) The concentration of captopril was determined by LC-MS using a standard curve.

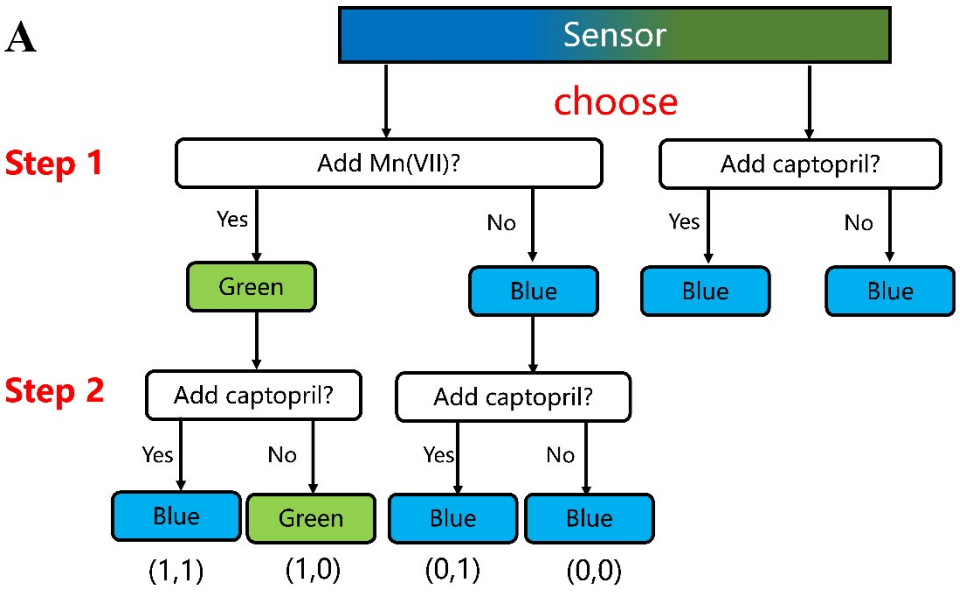

B

Input		Output		
Mn(VII)	Captopril	$F_{CDs}/F_{Fluorescein}$ (F_1/F_2)		
1	1	0	Blue emitting	
1	0	1	Green emitting	
0	0	0	Blue emitting	
0	1	0	Blue emitting	

C

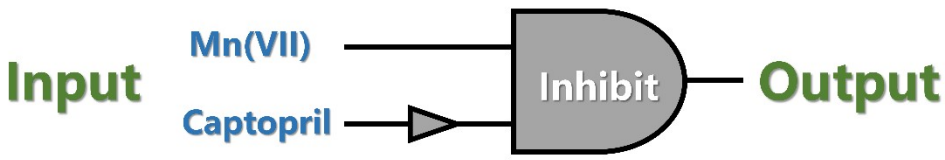

Figure S11. Design and operation of a fluorescent logic gate using the ratiometric fluorescent sensor. (A) Step-by-step diagram illustrating the operation of the fluorescent logic gate, which involves the addition of Mn(VII) and/or captopril to the sensor, followed by analysis of the fluorescent color and intensity using a smartphone-based system; (B) Truth table and QR codes for the logic gate operation parameters, which can be scanned and used to identify the inputs and outputs of the gate; (C) Simple logic gate diagram showing the inputs, and outputs.

Table S1. Comparison of different fluorescent probes for Mn(VII) detection

Comments	Precursors	Linear range (μM)	Detection limit (μM)	Reference
CQDs	Fresh loquat fruits	0.2-150	0.062	[1]
R-CDs	Malic acid Neutral red 1,8-diaminonaphthalene	0-115	0.0145	[2]
NS-CDs	Phosphoric acid Formamide	5-40	0.00716	[3]
Tb-TDA	2,5-thiophenedicarboxylic acid $Tb(NO_3)_3 \cdot 5H_2O$ Glacial acetic acid	0-200	0.612	[4]
N,S-CDs	Phthalic acid 1,2-ethylenediamine Concentrated phosphoric acid	10-200	0.0483	[5]
N-CDs	Auricularia auricula	0.15-9.00	0.12	[6]
Mn-CDs	Sulfanilicacid Manganese(II) Chloride Citric acid	3-150	0.66	[7]
NCD	p-hydroxybenzoic acid Ammonia	0.57-2	0.17	[8]
N-CQDs	m-phenylenediamine Grape seed powder	5-125	4.4	[9]
NCDs	Threonine Guanidine hydrochloride	5-35	0.66	[10]
NS-CDs	ascorbic acid Guanidine isothiocyanate	0.12-100	0.12	This work

Table S2. Comparison of different fluorescent probes for Captopril detection

Comments	Precursors	Linear range (μM)	Detection limit (μM)	Reference
CQDs	Citric acid Thiourea	1-50	0.1	[11]
N-CQDs	Polyethyleneimine Citric acid	10-65	0.00143	[12]
Fe/NC NZs	2-Methylimidazole Fe(acac)$_3$ $Zn(NO)_3 \cdot 6H_2O$	1-50	0.47	[13]
W, N-CDs	Diammonium citrate tris-(hydroxymethyl)-aminomethane Na_2WO_4	0.5-10	0.3	[14]
Cds-QDs	1,4-phenylene-N,N′ -bis (O,O-diphenylphoramidate) L-cysteine	0.05-90	0.015	[15]
CDs-AuNCs	Ethylenediamine Citric acid Glutathione $HuCl_4$	0.25-50	0.076	[16]
AgNCs	Glutathione $AgNO_3$	5-60	1.12	[17]
TTA-Tp COF	3,3’,5,5’-tetramethylbenzydine	1-100	0.78	[18]
Au@Cu-BTC	1,3,5-benzenetricarboxylate	0.5-7 10-2500	0.047	[19]
NS-CDs	ascorbic acid Guanidine isothiocyanate	0.52-300	0.52	This work

Table S3. Determination of Mn(VII) that added in medicinal herb samples (n=3).

Sample	Original/ μmol/L	Added/ μmol/L	Founded / μmol/L	Recovery (%)	RSD (%)
Ardisia crenata	1.46	10	11.19	97.30	8.20
		20	22.18	103.57	5.46
		30	29.59	93.78	1.51
Ardisia lindleyana	2.82	10	13.32	104.99	1.53
		20	24.30	107.39	1.64
		30	30.04	90.73	1.62
Schefflera Arboricola	1.14	10	11.41	102.68	3.30
		20	20.84	98.50	1.45
		30	28.61	91.57	0.34
Acanthopanax Senticosus	2.72	10	13.67	109.49	0.83
		20	23.36	103.22	1.11
		30	29.84	90.40	0.13
Glabrous Greenbrier Rhizome	3.28	10	13.61	103.27	1.82
		20	24.61	106.65	1.02
		30	30.67	91.30	0.14

Table S4. Determination of captopril that added in captopril tablet sample (n=3).

Sample	Original/ μmol/L	Added/ μmol/L	Founded / μmol/L	Recovery (%)	RSD (%)
Captopril tablet	91.13	60	153.30	103.61	2.78
		110	206.94	105.28	2.03
		200	282.23	95.55	3.31

Table S5. Determination of Mn(VII) by smartphones standard addition recovery (n=3).

Sample	Original/ μmol/L	Added/ μmol/L	Founded / μmol/L	Recovery (%)	RSD (%)	Color signal
Ardisia crenata	1.35 	10	11.41	100.61	6.98	
		20	22.16	104.07	5.25	
		30	31.80	101.50	3.56	
Ardisia lindleyana	2.72 	10	13.51	107.86	0.76	
		20	23.55	104.16	3.06	
		30	33.32	102.01	3.05	
Schefflera Arboricola	1.35 	10	11.05	97.04	1.16	
		20	22.80	107.24	1.82	
		30	33.06	105.71	1.18	
Acanthopanax Senticosus	2.82 	10	13.60	107.84	0.83	
		20	23.52	103.50	2.57	
		30	33.78	103.21	1.90	
Glabrous Greenbrier Rhizome	3.17 	10	13.55	103.76	0.43	
		20	24.09	104.57	2.77	
		30	32.65	98.28	1.97	

Table S6. Determination of captopril by smartphones standard addition recovery (n=3).

Sample	Original/ μmol/L	Added/ μmol/L	Founded / μmol/L	Recovery (%)	RSD (%)	Color signal
Captopril tablet	91.38 	60	152.43	101.75	1.80	
		110	202.37	100.90	3.56	
		200	290.82	99.72	0.25	

Reference

[1] P.Wang, J. Wang, T. Liu, Loquat fruit-based carbon quantum dots as an “ON-OFF” probe for fluorescent assay of MnO_4^- in waters based on the joint action of inner filter effect and static quenching, Microchem. J. 178 (2022) 107374.

[2] D. Chang, Z. Zhao, J. Feng, Lysosome-targeted red-fluorescent carbon dots for turn-on detection of permanganate and pH in vivo and in vitro, Sensor. Actuat. B-Chem. 349 (2021) 130774.

[3] L. Shi, J. Feng, X. Li, Handheld detection strategy: Real-time on-site assay of Mn(VII) and GSH integrating ratiometric fluorescent carbon dots paper strip, smartphones, and 3D-printed accessory, Actuat. B-Chem. 375 (2022) 132871.

[4] Z. Yuan, G. Hou, L. Han, A Terbium-Based MOF as fluorescent probe for the detection of Malachite Green, Fe^{3+} and MnO_4^-, Zeitschrift für anorganische und allgemeine Chemie 648 (2021) e202100301.

[5] F. Du, G. Li, X. Gong, Facile, rapid synthesis of N,P-dual-doped carbon dots as a label-free multifunctional nanosensor for Mn(VII) detection, temperature sensing and cellular imaging, Actuat. B-Chem. 277 (2018) 492-501.

[6] W. Chen, H. Lin, Y. Wu, Fluorescent probe of nitrogen-doped carbon dots derived from biomass for the sensing of MnO_4^- in polluted water based on inner filter effect, Adv. Compos. Hybrid. Ma. 5 (2022) 2378-2386.

[7] X. Chu, G. Ning, Z. Zhou, Bright Mn-doped carbon dots for the determination of permanganate and L-ascorbic acid by a fluorescence on-off-on strategy, Microchim. Acta. 187 (2020) 659.

[8] V. Naik, D. Gunjal, A. Gore, Nitrogen-doped carbon dot threads as a "turn-off" fluorescent probe for permanganate ions and its hydrogel hybrid as a naked eye sensor for gold (III) ions, Anal. Bioanal. Chem. 412 (2020) 2993-3003.

[9] L. Lin, Q. Lai, Q. Chen, Turning waste into wealth: nitrogen-doped carbon quantum dots derived from fruits wastes for sensing, Luminescence (2021) 37340-347.

[10] A. Mohammed, Y. Gugulothu, R. Bandi, Ultraspeed synthesis of highly fluorescent N-doped carbon dots for the label-free detection of manganese (VII), J. Chin. Chem. Soc-Taip. 68 (2021) 1514-1521.

[11] Y. Fu, Z. Li, Z. Zhou, A Fluorescent Self-Absorption Method for Detection of Captopril using Carbon Quantum Dots, Chemistryselect. 7 (2022) e202200518.

[12] L. Dewangan, Y. Chawre, J. Korram, N-doped, silver, and cerium co-doped carbon quantum dots based sensor for detection of Hg^{2+} and captopril, Microchem. J. 182 (2022) 107867.

[13] M. Wu, Y. Lv, Z. Lin, Dual-mode colorimetric and fluorescence sensing system for the detection of captopril based on Fe/NC nanozymes and carbon dots, Spectrochim. Acta. A. 282 (2022) 121683.

[14] Y. Guan, Y. Zu, P. Ma, Cascade Fluorescent Determination of Mercury (II) and Captopril Using Tungsten-Nitrogen Doped Carbon Dots, Anal. Lett. 2023.

[15] G. Paimard, M. Gholivand, M. Shamsipur, Fabrication of a highly sensitive amperometric

sensor using 1,4-phenylene-N,N′-bis (O,O-diphenylphoramidate)/CdS quantum dots/multi-walled carbon nanotubes for nanomolar detection of captopril, J. Electroanal. Chem. 738 (2015) 176-183.

[16] L. Han, T. Liu, D. Cui, Quantitative detection of captopril in urine by smartphone-assisted ratiometric fluorescence sensing platform, Spectrochim. Acta. A. 280 (2022) 121562.

[17] L. Xi, X. Zhang, Y. Chen, A fluorescence turn-on strategy to achieve detection of captopril based on Ag nanoclusters, Chem. Phys. Lett. 807 (2022) 140085.

[18] M. Yuan, S. Xiao, Y. Wu, Visual detection of captopril based on the light activated oxidase-mimic activity of covalent organic framework, Microchem. J. 175 (2021) 107080.

[19] D. Silva, M. Areias, Detection of Captopril in a Commercial Drug Using a Gold-Copper Metal-organic Framework Nanocomposite Modified Electrode, Electroanal. 33 (2021) 1255-1263.